# MAGNETIC RECONNECTION IN THE CORONA AND THE LOOP PROMINENCE PHENOMENON

R. A. KOPP* and G. W. PNEUMAN
*High Altitude Observatory, National Center for Atmospheric Research,† Boulder, Colorado* 80303

(Received 3 May, 1976)

**Abstract.** Many classes of transient solar phenomena, such as flares, flare sprays, and eruptive prominences, cause major disruptions in the magnetic geometry of the overlying corona. Typically, the results from Skylab indicate that pre-existing closed magnetic loops in the corona are torn open by the force of the disruption. We examine here some of the theoretical consequences to be expected during the extended relaxation phase which must follow such events. This phase is characterized by a gradual reconnection of the outward-distended field lines. In particular, the enhanced coronal expansion which occurs on open field lines just before they reconnect appears adequate to supply the large downward mass fluxes observed in H$\alpha$ loop prominence systems that form during the post-transient relaxation. In addition, this enhanced flow may produce nonrecurrent high speed streams in the solar wind after such events. Calculations of the relaxation phase for representative field geometries and the resulting flow configurations are described.

## 1. Introduction

Loop prominence systems, usually seen after major flares (Bruzek, 1964), are one of the most beautiful and yet least understood phenomena observed on the surface of the Sun. Beginning minutes after the onset of the flare, they are seen in H$\alpha$ as cool material streaming downward toward the chromosphere on both sides of the loop. The loop pattern expands upward at a velocity of 10–20 km $s^{-1}$ and is generally imbedded in a hot coronal condensation, visible in $\lambda$5303 and other high-temperature coronal emission lines. The visual impression of this expansion is that individual magnetic flux tubes remain stationary, and that loops at progressively higher levels of the atmosphere become illuminated at different times (Bruzek, 1964; Kleczek, 1964). The H$\alpha$ material is already in motion when it first becomes visible, descending with approximately the gravitational free-fall speed. The typical post-flare loop system lasts about ten hours, and the total mass delivered to the chromosphere is $10^{15}$–$10^{16}$ gm (Kleczek, 1964).

Condensation of prominence material from the hot corona immediately surrounding the prominence has been suggested by many authors to explain the origin of ordinary quiescent prominences (Kiepenheuer, 1951, 1953, 1959; Orrall and Zirker, 1961, 1963; Menzel and Doherty, 1963). However, this process is clearly inadequate to explain loop prominence systems, in which the total mass observed streaming downward considerably exceeds the total mass of the associated coronal condensation (Jefferies and Orrall, 1963a,b, 1965; Kleczek, 1963, 1964). Moreover, considering the high electrical conductivity of the coronal

* New address: Los Alamos Scientific Laboratory, Los Alamos, N.M. 87545, U.S.A.
† The National Center for Atmospheric Research is sponsored by the National Science Foundation.

*Solar Physics* **50** (1976) 85–98. 

plasma, it is difficult to explain how material from the corona crosses the lines of force to enter the prominence. Thermalization of energetic particles emanating from the flare region and stored in the corona has also been suggested (Jefferies and Orrall, 1964, 1965; Newkirk, 1973). However, in this case inordinately strong magnetic fields are needed in the prominence to contain the required number of particles.

In this paper we propose an alternative mechanism – namely, that the post-flare loop prominence systems are *a result of the reconnection of magnetic field lines torn open by the flare outburst.* The sudden outward distantion of closed field lines during solar transient events has been commonly observed during the Skylab mission (MacQueen *et al.*, 1974). The mass is supplied to the prominence region by the capture of enhanced solar wind outflow which occurs as these field lines are transformed, via reconnection, to a closed configuration once again. The apparent expansion of the loop system is one manifestation of the reconnection process, proceeding upward into the corona and forming new closed loops at successively higher levels. In the following sections we will show that both the cool prominence and hot condensation can be understood in the context of a *continuous flow process* which is inevitably set up to restore the original magnetic configuration disrupted by the transient expulsion, and that this process can supply the mass required to sustain the prominence system during its lifetime.

## 2. Coronal Expansion on Moving Magnetic Flux Tubes

Figure 1 schematically shows two phases of the loop formation process of interest here. We suppose that, prior to the transient, the magnetic configuration of the corona overlying the flare site contains many closed loops. The material is of high density and the pressure, gravitational, inertial, and magnetic forces are initially in balance (Pneuman and Kopp, 1971). Through the sudden release of mass and

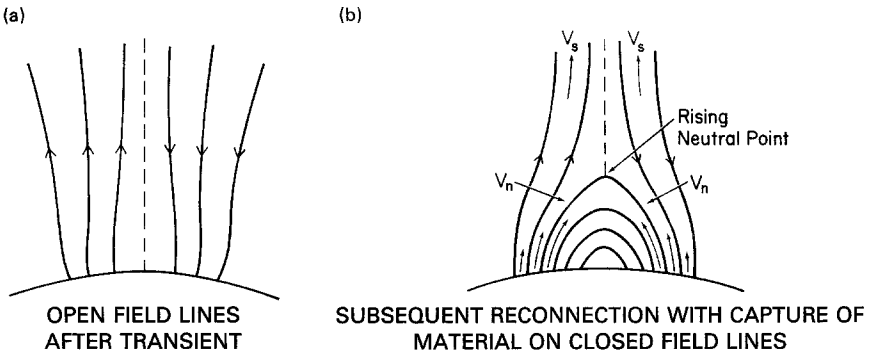


Fig. 1. Post-transient field configuration. (a) Bipolar open field configuration with neutral sheet produced by the force of the transient. (b) Rising loop system during reconnection phase following the transient. $V_s$ is the solar wind velocity along the open field lines, while $V_n$ denotes the velocity of the field lines themselves as they move towards the rising neutral sheet separating fields of opposite polarity.

energy the flare event then tears open the field lines into a configuration such as in Figure 1a – an open bipolar field geometry with a magnetic neutral sheet. A solar wind expansion is soon set up and the resulting losses tend to reduce the pressure below that which existed in the disruptive phase (Pneuman, 1973). Consequently, there arises an inward magnetic force towards the neutral sheet which can no longer be balanced by pressure forces. This unbalanced Lorentz force drives field lines towards the neutral sheet, and reconnection begins to take place proceeding upwards from the coronal base. At any given instant of time during this phase, the configuration will appear as in Figure 1b with open lines transforming into closed lines at a rising neutral point. The neutral point will continue to rise until the original configuration before the flare is restored (assuming no other changes in boundary conditions have occurred meanwhile).

If we consider the changes in any given flux tube during this process, we see that its geometry is altered drastically as a function of time. These changes in geometry have a profound effect on the flow dynamics within the tube. Beginning with approximately radial outflow as in Figure 1a, the expansion is affected by centrifugal and Coriolis forces and by cross-sectional changes as the tube 'swings' over towards the neutral point. This motion, it will be shown, increases the outward velocity markedly – especially in the last moments before the tube closes. When the flux tube closes, all the material below the neutral point is captured in the closed region. In addition, material continues to flow upward into the closed region until a sonic disturbance (or shock) travels from the neutral point down to the coronal base, causing the expansion to cease.* This shock raises the temperature of the coronal gas up to $3\text{–}4\times10^6$ K and forms the condensation. Subsequent rapid radiative cooling of this compressed gas produces the H$\alpha$ prominence, while new condensation material is being generated on higher loops. We shall return to these points in more detail in Section 4. We now wish to formulate the basic equations applicable to coronal expansion on moving flux tubes.

If we write the component of the momentum equation along the field, the $\mathbf{J}\times\mathbf{B}$ force, of course, does not enter and we have

$$\hat{e}_s \cdot \left[\frac{\partial \mathbf{V}}{\partial t} + (\mathbf{V}\cdot\nabla)\mathbf{V}\right] = -\frac{1}{\rho}\frac{\partial P}{\partial s} - \frac{GM_\odot}{r^2}\,\hat{e}_r \cdot \hat{e}_s\,, \tag{1}$$

where $\mathbf{V}$ is the velocity vector, $\rho$ the density, $P$ the gas pressure, $G$ the gravitational constant, $M_\odot$ the solar mass, and $r$ the radial distance from the center of the Sun. $\hat{e}_r$ and $\hat{e}_s$ are respectively unit vectors in the radial direction and in a direction along a field line. In order to illustrate the relevant physics, it will be sufficient here to restrict the discussion to meridional field configurations which

* This process is similar to that which is believed to occur in the earth's mid-latitude magnetic field lines following geomagnetic storms. There, material flowing upward supersonically from the topside ionsphere to refill flux tubes depleted during the storm is subsequently brought to rest by a downward propagating shock wave (Banks *et al.*, 1971).

are axisymmetric about the Sun. Then **V** can be written in the form

$$\mathbf{V} = V_s\hat{e}_s + V_n\hat{e}_n,$$

where $V_s$ is the component of the fluid velocity along the field line and $V_n$ the component perpendicular to the field. $\hat{e}_n$ is a unit vector in the meridional plane normal to the field. Noting that the relevant derivatives of the unit vectors are:

$$\frac{\partial\hat{e}_s}{\partial t} = \hat{e}_n\frac{\partial\alpha}{\partial t}; \quad \frac{\partial\hat{e}_n}{\partial t} = -\hat{e}_s\frac{\partial\alpha}{\partial t}$$

$$\frac{\partial\hat{e}_s}{\partial s} = \hat{e}_n/R; \quad \frac{\partial\hat{e}_n}{\partial s} = -\hat{e}_s/R$$

$$\frac{\partial\hat{e}_s}{\partial n} = \hat{e}_n/R_n; \quad \frac{\partial\hat{e}_n}{\partial n} = -\hat{e}_s/R_n,$$

where $R$ is the radius of curvature of the field line, $R_n$ the radius of curvature of the field line normal, and $\alpha$ the angle between the field line and the radius vector, we can now write Equation (1) in the form:

$$\frac{\partial V_s}{\partial t} + V_s\frac{\partial V_s}{\partial s} + V_n\frac{\partial V_s}{\partial n} =$$

$$= -\frac{1}{\rho}\frac{\partial P}{\partial s} - \frac{GM_\odot}{r^2}\cos\alpha + V_n\frac{\partial\alpha}{\partial t} + \frac{V_nV_s}{R} + \frac{V_n^2}{R_n}. \qquad (2)$$

In the above equations, the time derivative $\partial/\partial t$ and the spatial derivatives $\partial/\partial s$ and $\partial/\partial n$ refer to changes as seen by a fixed observer. It is convenient to define new derivatives which will denote changes as seen by an observer *fixed* on a given field line, i.e., an observer who moves with the field line normal to itself ($ds = 0$). These derivatives will be noted by the symbols $D/Dt$ and $D/Ds$. It can then easily be shown that

$$\frac{\partial V_s}{\partial t} = \frac{DV_s}{Dt} - V_n\frac{\partial V_s}{\partial n}$$

$$\frac{\partial V_s}{\partial s} = \frac{DV_s}{Ds}$$

and

$$\frac{\partial\alpha}{\partial t} = \frac{D\alpha}{Dt} - V_n\frac{\partial\alpha}{\partial n}.$$

Finally, using the geometrical relation

$$\frac{1}{R_n} = \frac{\partial\alpha}{\partial n} + \frac{\cos\alpha}{r}$$

we obtain

$$\frac{DV_s}{Dt}+V_s\frac{DV_s}{Ds}=-\frac{1}{\rho}\frac{DP}{Ds}-\frac{GM_\odot}{r^2}\cos\alpha+V_n\frac{D\alpha}{Dt}+\frac{V_n^2}{r}\cos\alpha+\frac{V_nV_s}{R}. \tag{3}$$

Similar manipulations on the continuity equation yield

$$\frac{D}{Dt}(\rho A)+\frac{D}{Ds}(\rho V_sA)-\frac{\rho V_nA}{R}=0, \tag{4}$$

where $A$ is the cross-sectional area of the flux tube. The last term in Equation (4) represents the dilatation of an infinitesimal length of the flux tube as it moves normal to itself. This will always occur if the tube is curved.

Equations (3) and (4) are normally complemented by an appropriate energy equation relating the pressure, $P$, and density, $\rho$. For simplicity, we have assumed in the present work that the plasma flow is isothermal and that $P$ and $\rho$ are related by the perfect gas law

$$P=\rho c^2,$$

where $c^2=kT/m$ is the isothermal sound speed, $k$ is Boltzmann's constant, and $m$ is the mean particle mass ($=m_p/2$ for ionized hydrogen).

Equations (3) and (4) are especially convenient forms of the fluid equations for problems in which the stream tube geometry (here defined by the magnetic field) is prescribed as a function of time, for they allow the flow to be determined along each flow tube separately. For a known stream-tube geometry, Equations (3) and (4) comprise two coupled first-order partial differential equations for $P$ and $V_s$ in terms of $s$ and $t$. It is easily shown that they are a hyperbolic set; thus they may be solved numerically by the method of characteristics.

Consider the application of Equations (3) and (4) to determine the flow $V_s(s, t)$ and $P(s, t)$, *on specific flux tube*, whose motion, as prescribed by $V_n$, $\alpha$, $R$, and $A$, is known as a function of time. Combining these relations in the usual manner yields the equivalent set of characteristic equations:

$$\left.\frac{d\xi}{dt}\right|_{C^+}=-V_s\frac{\partial lnA}{\partial s}-\frac{\partial lnA}{\partial t}-\frac{GM_\odot}{r^2c}\cos\alpha+\frac{V_n}{c}\frac{\partial\alpha}{\partial t}+\frac{V_n^2}{cr}\cos\alpha, \tag{5}$$

$$\left.\frac{d\eta}{dt}\right|_{C^-}=-V_s\frac{\partial lnA}{\partial s}-\frac{\partial lnA}{\partial t}+\frac{GM_\odot}{r^2c}\cos\alpha-\frac{V_n}{c}\frac{\partial\alpha}{\partial t}-\frac{V_n^2}{cr}\cos\alpha, \tag{6}$$

where $\xi=\ln P+V_s/c$ and $\eta=\ln P-V_s/c$. The time derivatives appearing on the left-hand sides of these expressions are taken along the positive ($C^+$) and negative ($C^-$) characteristics, respectively, the directions of which in the $s, t$-plane are given by

$$\frac{ds}{dt}=V_s+c \quad \text{along } C^+ \tag{7}$$

and

$$\frac{ds}{dt} = V_s - c \quad \text{along } C^-. \tag{8}$$

In carrying out a numerical solution of this system of equations, a network of characteristics, along which Equations (5) and (6) apply, evolves with time along with the actual solution for $\xi$ and $\eta$ (or, equivalently, $P$ and $V_s$).

Special attention must be given to the specification of boundary conditions in problems involving time-dependent flows, to insure that the solution be uniquely determined. The necessary and sufficient conditions which must be prescribed at the boundaries of our flow region are most readily determined from the theory of characteristics: in addition to specifying the initial dynamical state $P(s)$ and $V_s(s)$ at $t=0$, the number of independent relations between $P$ and $V_s$ which must be specified at any spatial boundary is $2-n$, where $n$ is the number of characteristics crossing each point of that boundary from the interior of the solution in the direction of increasing time. In the case at hand, the flow at the lower boundary (coronal base) will be seen to be subsonic at all times; as $t$ increases information reaches this boundary from the solution domain ($r > r_0$) only along the negative characteristics. That is, the values of $\eta$ at the inner boundary, communicated from the interior of the solution to that boundary via Equation (6), constitute a time-varying functional constraint, $\eta_0(t)$, between the boundary values $P(s_0)$ and $V_s(s_0)$. Only one additional relationship between these quantities can be imposed there. For the calculations in this paper, we have chosen to keep the pressure at the coronal base, $P(s_0)$, fixed with time. This condition, combined with the above constraint imposed by $\eta_0(t)$, determines the run of base velocity, $V_s(s_0)$, with time.

By placing the outer boundary of the flow far enough from the Sun to insure that the expansion is always supersonic there, both positive and negative characteristics cross that boundary toward increasing time. Thus, both $\xi$ and $\eta$ are determined at the boundary by the evolution of the flow closer to the Sun, and no additional constraints can be imposed on the flow there.

## 3. A Numerical Example

The previous section described how the time-dependent expansion can be calculated in a single moving flux tube. We now wish to expand these results to a collection of flux tubes such as might be expected to take part in the reconnection process. If $r_1(t)$ represents the position of the rising neutral point, then a suitable magnetic configuration contains closed loops extending up to $r_1(t)$ with open lines adjacent to and above the loops. For $r < r_1(t)$, a simple field geometry which has all the desired characteristics can be constructed by superposing a solar-centered dipole field and a uniform field parallel to the Sun's rotation axis, with the relative strengths chosen to make the field become radial at $r = r_1(t)$. The radial

and transverse components of this field are given by

$$B_r = \left\{\frac{1+2\left[\frac{r_1(t)}{r}\right]^3}{1+2\left[\frac{r_1(t)}{r_0}\right]^3}\right\}\cos\theta$$

$$B_\theta = -\left\{\frac{1-\left[\frac{r_1(t)}{r}\right]^3}{1+2\left[\frac{r_1(t)}{r_0}\right]^3}\right\}\sin\theta, \qquad r_0 \leqslant r \leqslant r_1(t), \tag{9}$$

where $r_0$ is some reference level, here chosen to be the coronal base. The field at greater heights is taken to be the radial extension of the field at $r_1$ given by Equations (9), i.e.,

$$B_r = \frac{3\left[\frac{r_1(t)}{r}\right]^2}{1+2\left[\frac{r_1(t)}{r_0}\right]^3}\cos\theta \quad r \geqslant r_1(t) \tag{10}$$

$$B_\theta = 0.$$

When $r_1(t) = r_0$, the field is purely radial, but as $r_1$ increases closed loops are formed below the neutral point, giving a picture at some later time such as that shown in Figure 2. If we now let $r_1(t)$ increase with time from $r_0$ to some equilibrium position $r_e$, we can effectively model the entire reconnection process, beginning with a purely radial open field and ending with a stable helmet streamer containing closed field below the neutral point and open lines above and outside the closed region. For our example we shall take $r_1$ to be of the form

$$r_1(t) = r_e - (r_e - r_0)e^{-\omega t}, \tag{11}$$

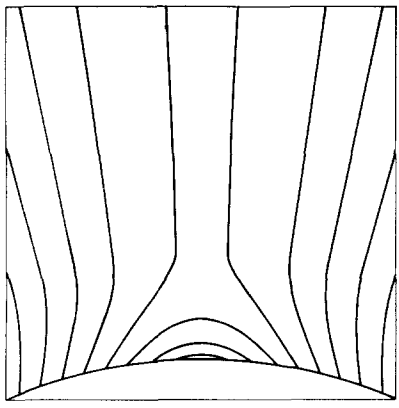

Fig. 2. Typical field configuration calculated from Equations (9) and (10). In this figure, reconnection from a purely radial field has proceeded for 3 hours in accordance with Equation (11).

where $\omega^{-1}$ corresponds to the time scale of the reconnection phase. Here, we will choose $r_0 = R_\odot$ and $r_e = 1.5\, R_\odot$, consistent with the observed heights of closed loops in typical helmet streamers. Also in our model, we identify the observed rate of growth of the post-flare loop system with the velocity at which the neutral point rises during the reconnection process; i.e., we choose $\omega$ so that the neutral point velocity, $dr_1/dt$, is 20 km s$^{-1}$ at $r = r_0$. This gives $\omega = 5.7 \times 10^{-5}$ s$^{-1}$.

Equations (5) through (8) are now to be intergrated along individual flux tubes subject to a specified boundary condition at the base of each tube. Physically, we expect the gas pressure at the base to remain approximately invariant since a violation of this condition would seriously affect hydrostatic equilibrium conditions in the denser underlying layers. Since we are assuming isothermal conditions, this means that the density at the base will likewise remain fixed. In the following, we will fix the density at the base of each flux tube at a value independent of latitude. For the calculation, the actual value of the base density is irrelevant. In order to integrate Equations (5)–(8), the geometrical quantities describing the field and its motion must also be specified. These are easily found from the expressions (9) and (10). Letting $x = r/r_0$ and $x_1(t) = r_1(t)/r_0$ we obtain

$$\alpha(x, t) = \tan^{-1}\left[\left(\frac{x^3 - x_1^3}{x^3 + 2x_1^3}\right)\tan\theta\right] \tag{12}$$

$$V_n(x, t) = \left(\frac{3x_1^2 x}{1 + 2x_1^3}\right)\left(\frac{x^3 - 1}{x_1^3 - x^3}\right)\frac{dx_1}{dt}\, r_0 \sin\alpha \tag{13}$$

$$R(x, t) = \left\{\frac{\cos^2\alpha \sin\alpha}{x^3 + 2x_1^3}\left[\left(\frac{9x_1^3 x^2}{x^3 - x_1^3}\right) - \left(\frac{x^3 - x_1^3}{x}\right)(1 + \tan^2\theta)\right] + \frac{\sin\alpha}{x}\right\} r_0 \tag{14}$$

for $x \leqslant x_1(t)$ and

$$\alpha(x, t) = 0 \tag{15}$$

$$V_n(x, t) = \frac{x_1^3 - 1}{1 + 2x_1^3}\left(\frac{x}{x_1}\right)\frac{dx_1}{dt}\, r_0 \tan\theta \tag{16}$$

$$R(x, t) = \infty \tag{17}$$

for $x \geqslant x_1(t)$. The instantaneous cross-sectional area of the flux tube can be evaluated directly from Equations (9) and (10), using the expression

$$A(x, t) = B_0 A_0 / B(x, t), \tag{18}$$

where $B_0$ and $A_0$ are, respectively, the field strength and area at the base of the flux tube. In the above equations, $x_1(t)$ and $dx_1/dt(t)$ are evaluated from Equation (11).

In order to illustrate the physical properties of the solution, consider the time variation of the velocity distribution along a single flux tube as it participates in the

reconnection process – keeping in mind that the complete two-dimensional picture will be a composite of solutions along neighboring tubes as well. Referring to Figure 1, we see that an arbitrarily chosen tube is approximately radial as the reconnection begins. As the neutral point rises, the tube bends towards the center (the footprint remaining fixed) and forms a closed loop when it meets the arising neutral point at the center. Note from Equations (13), (16), and (18), that both $V_n$ and $A$ become large without limit just as the tube closes. This is due to the fact that the magnetic field vanishes as the neutral point is approached.* This characteristic leads to two important physical effects which tend to increase the outward velocity along the tube. Firstly, the outward centrifugal force, $\rho V_n^2/R$ becomes large. Secondly, and most importantly, the rapid spreading of the cross section just before the tube closes produces a dramatic decrease in the density in the vicinity of the neutral point. As a result, the expansion along the tube 'feels' an essentially zero pressure at a finite distance rather than at infinity such as would be the case for a fixed tube. Thus, the 'effective' outward pressure gradient becomes much larger leading to a corresponding increase in the flow velocity.

The calculated velocity distribution along such a typical flux tube as the neutral point rises into the corona is shown in Figure 3. Starting from the bottom of the figure and proceeding upward, the curves show the velocity variation with radial distance along the tube at successively later times during the reconnection process. This particular tube closes when the neutral point reaches a radial distance of 1.2 $R_\odot$. Since the tube is initially radial, the bottom curve is just the

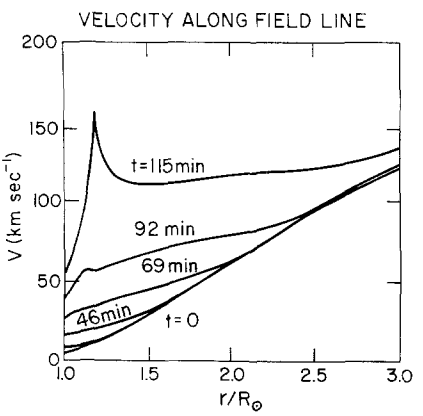


Fig. 3. Velocity as a function of radial distance along a typical flux tube of Figure 2 during successive stages of the reconnection process. The bottom curve represents the initial velocity profile, which is simply the Parker isothermal solution for radial flow. Proceeding upward in the figure, the curves show how the velocity distribution changes with time as the tube approaches the neutral sheet. The enhanced flow at $t = 115$ min. occurs just before this field line closes, with the spike in the profile being produced near the the neutral point at $r = 1.2\ R_\odot$.

* It should be noted here that this is a general characteristic only for potential fields containing a $Y$-type neutral point. For a cusp-type neutral point, such as might occur in the MHD case (Pneuman and Kopp, 1971), $V_n$ and $A$ increase but remain finite.

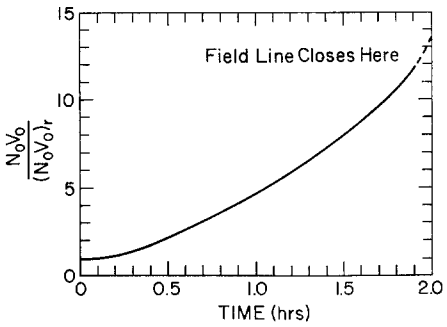


Fig. 4. Ratio of the particle flux at the coronal base to that for radial flow as a function of time for the flux tube described in the caption of Figure 3. Note that, just as the field line closes, the mass flux into the tube is enhanced by a factor of 12 over that predicted for a radial solar wind.

radial isothermal solar wind solution first derived by Parker (1958). Proceeding in time, the velocity first increases between the base and the neutral point, with the increase spreading outward along the tube with the speed $V_s + c$. A 'spike' in the velocity distribution then begins to appear at the height where this particular field line meets the neutral point (1.2 $R_\odot$). The top curve shows the velocity just before the tube closes. Note that the speed near the neutral point has increased to about 160 km $s^{-1}$ – about 16 times the Parker value. The velocity at the base has also increased from just a few km $s^{-1}$ to about 60 km $s^{-1}$. In addition, a broad high velocity region has grown outside the neutral point which extends well out into the corona. It is shown in another paper (Pneuman and Kopp, 1976) that this high velocity 'tail' persists long after the reconnection has ceased (about a day) and may extend out to the orbit of Earth – providing a possible explanation for the non-recurrent high speed streams often observed following major solar flares (Hundhausen *et al.*, 1970).

In Figure 4 we have plotted the ratio of the particle flux at the base of this flux tube to that for radial flow as a function of time. Note that, just as the flux tube closes, the particle flux has increased by a factor of about 12 over its initial value. When the field line closes (after about 2 hours) the material just below the neutral point is immediately brought to rest, forming a downward propagating shock wave. Mass continues to flow into the tube, however, until this shock reaches the coronal base, signaling the entire flow process to cease. Taking $V_0 = 60$ km $s^{-1}$ from Figure 3, $N_0 = 10^{10}$ $cm^{-3}$ and assuming the shock travels downward at approximately the sound speed, the mass per $cm^2$ of base area accumulated in the tube after closing will be $10^{-7}\, h/c$ where $h$ is the height of the tube and $c$ is the sound speed. Taking the average height of the entire loop system to be 0.2 $R_\odot$ with a base area of $10^{19}$ $cm^2$ and a sound speed of 150 km $s^{-1}$ characteristic of coronal temperatures, the total mass delivered to the prominence system is $\approx 10^{15}$ gm. This estimate is in good agreement with that observed falling as visible H$\alpha$ material (Kleczek, 1964).

## 4. Discussion

Let us now extend the results for a single flux tube discussed in Section 3 to the prominence system as a whole. The discussions of this section will center around Figure 5, which is a schematic of the entire loop system showing several flux tubes, each at a different stage of the reconnection process. As the reconnection proceeds upward, each tube passes successively through the three stages as are shown on the figure, i.e., all three conditions are present in the corona during the entire process but occur always on different flux tubes. We describe each stage in some detail in the following paragraphs:

(1) *Coronal condensation.* The coronal condensation is maintained on the most recently closed flux tubes. Immediately upon closing (within a few collision times), a downward propagating shock is set up on these tubes heating and compressing the gas behind. The shock Mach number is given by

$$M-\frac{1}{M}=\frac{\gamma+1}{2}\left(\frac{V_1-V_2}{c}\right),$$

where $V_1$ is the velocity of the upward moving unshocked material, $V_2$ is the velocity behind the shock. Our calculations show that the flow just before the flux tube closes is approximately sonic at the neutral point (see Figure 3), hence $V_1 \approx c$. Since the flow is assumed to be brought to rest by the shock, $V_2 = 0$. This gives us a Mach number of about 1.9 for $\gamma = \frac{5}{3}$. The density and temperature ratios are then

$$\frac{N_2}{N_1}=\frac{(\gamma+1)M^2}{(\gamma-1)M^2+2}\approx 2.2$$

$$\frac{T_2}{T_1}=1+\frac{2(\gamma-1)}{(\gamma+1)^2}\frac{\gamma M^2+1}{M^2}(M^2-1)=1.8.$$

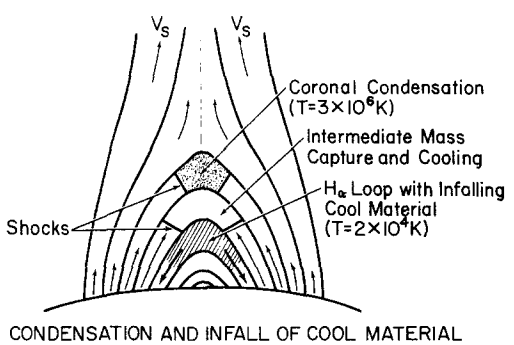


Fig. 5. Schematic of the entire loop prominence system during the reconnection process. Here, each closed loop passes successively through three stages: (1) the hot compressed region which forms on the most recently closed tubes, here identified with the coronal condensation; (2) intermediate phase in which mass continues to cool radiatively and begins to fall; and (3) the H$\alpha$ phase where the material has cooled to temperatures in the range $10^4$–$10^5$ K and continues to fall towards the chromosphere. The arrows in the figure depict the direction of the flow.

Thus, if the unshocked material is at coronal temperatures ($1.5–2\times10^6$ K), the temperature of the condensation behind the shock will be $3–4\times10^6$ K. This compressed gas now begins to cool while new condensation material is being formed above it.

(2) *Intermediate.* As the reconnection proceeds, the gas continues to accumulate on the lower closed lines until the shock reaches the base of the corona. It now begins to cool radiatively from the condensation temperatures and becomes invisible in the green and yellow lines but is still too hot to be observed in H$\alpha$. To estimate the radiative cooling time, we assume that the time rate of energy decrease due to radiative losses is (Cox and Tucker, 1969)

$$\frac{dE}{dt}=6\times10^{-22}N_e^2\ ,$$

where $E$ is the energy density of the gas and $N_e$ is the electron density. Taking $E=3N_ekT$, we have crudely

$$\frac{dE}{dt}=\frac{d}{dt}(3N_ekT)\approx\frac{3N_ekT}{t_r}=6\times10^{-22}N_e^2,$$

where $t_r$ is the radiative relaxation time. Hence $t_r=5\times10^{21}kT/N_e$ and is about $\frac{1}{2}$ hour for a condensation temperature of $3\times10^6$ K and density of $10^9$ cm$^{-3}$. As the temperature falls the scale height is reduced and there is soon (within one radiative cooling time) too much material in the loop to be supported against gravity by the pressure gradient. The gas then begins to fall along the loop towards the chromosphere under the acceleration of gravity.

(3) H$\alpha$ *loops.* If the material is still at coronal heights by the time that it has cooled down to temperatures in the range $10^4$–$10^5$ K, it becomes visible in H$\alpha$. It is, of course, already falling when this occurs. For this reason, it is difficult to estimate the total amount of mass released by a given loop from H$\alpha$ observations alone. Depending on the density of the captured material, it is even possible that certain events may produce no H$\alpha$ manifestation at all, or that H$\alpha$ emission will be appreciable only near the footpoints of the flux tube (coronal rain), just before impact of the material on the chromosphere. Possible candidates for events of this type are the rising loop structures seen only in soft X-rays during the ATM mission (Webb *et al.*, 1976).

## 5. Summary

In this paper we have proposed that the rising loop prominence systems often seen after major solar flares and coronal transients are the result of magnetic field reconnection in the corona. The reconnection process is visualized as the closing of field lines previously torn by the transient event. When the field is opened a

solar wind expansion is set up, which subsequently provides mass for the prominence system as open lines are transformed into closed lines by reconnection. Time-dependent calculations of the expansion as the field lines move during this process show that, just before a flux tube closes, the upward mass flow is enhanced by as much as a factor of 10 over that predicted for stationary radial flow. This material captured on the closed loops, in addition to that which continues to flow into the loop for some time after closing, can adequately account for the $10^{15}$ gm observed in H$\alpha$ falling towards the chromosphere during the lifetime of the prominence.

The hot coronal condensation associated with the prominence system is formed on the most recently closed loops by a downward propagating shock wave, which brings the flow to rest and heats the gas to temperatures of $3\text{–}4\times10^6$ K. The material begins to fall along the loop within the first radiative cooling time after the field line closes. For sufficiently dense loops radiative cooling is fast enough that temperatures as low as $10^4\text{–}10^5$ K are reached before the gas has exited the loop to the chromosphere. For these loops the H$\alpha$ phase is the final stage of the loop prominence model developed here. During this process new condensation material is being formed on higher loops. Thus, the loop prominence phenomenon should be viewed as a sequential flow process with any given stage (e.g., condensation, H$\alpha$ phase, etc.) occurring on progressively higher field lines. According to this picture, the total amount of mass represented by the loop prominence system over its lifetime need not be in the corona at one time. Thus, the traditional problem of explaining the origin of the prominence material disappears.

## Acknowledgements

The authors are indebted to Dr Frank Orrall for several discussions of the post-flare loop phenomenon, to Dr Eric Priest for discussion of the reconnection problem, and to Mrs Sara Martin for pointing out that the reconnection model presented here may also apply to the loop structures observed only in soft X-rays (Webb *et al.*, 1976) following certain flares and eruptive prominences.

## References

Banks, P. M., Nagy, A. F., and Axford, W. I.: 1971, *Planet. Space Sci.*, **19,** 1053.

Bruzek, A.: 1964, in W. Hess (ed.), *AAS-NASA Symposium on the Physics of Solar Flares,* Washington, D.C.

Cox, D. P., and Tucker, W. H.: 1969, *Astrophys. J.* **157,** 1157.

Hundhausen, A. J., Bame, S. J., and Montgomery, M. D.: 1970, *J. Geophys. Res.* **75,** 4631.

Jefferies, J. T., and Orrall, F. Q.: 1963a, "*The Solar Spectrum*", Utrecht.

Jefferies, J. T., and Orrall, F. Q.: 1963b, *Astrophys. J.* **137,** 1232.

Jefferies, J. T., and Orrall, F. Q.: 1964, in W. Hess (ed.), *AAS-NASA Symposium on the Physics of the Solar Flares,* Washington, D.C.

Jefferies, J. T., and Orrall, F. Q.: 1965, *Astrophys. J.* **141,** 519.

Kiepenheuer, K. O.: 1951, *Pub. A.S.P.* **63,** 161.
Kiepenheuer, K. O.: 1953, *Acad. Naz. d. Lincei, Convegno Volta* **11,** 148.
Kiepenheuer, K. O.: 1959, *Zs. f. Ap.* **48,** 290.
Kleczek, J.: 1963, *Bull. Astr. Inst. Czechoslovakia* **14,** 167.
Kleczek, J.: 1964, in W. Hess (ed.), *AAS-NASA Symposium on the Physics of Solar Flares,* Washington, D.C.
MacQueen, R. M., Eddy, J. A., Gosling, J. T., Hildner, E., Munro, R. H., Newkirk, G. A., Jr., Poland, A. I., and Ross, C. L.: 1974, *Astrophys. J.* **187,** L85.
Menzel, D. H., and Doherty, L. R.: 1963, in J. W. Evans (ed.), 'The Solar Corona', *IAU Symp.* **16.**
Newkirk, G. Jr.: 1973, in R. Ramaty and R. G. Stone (eds.), *Symposium on High Energy Phenomena on the Sun,* NASA Goddard Spaceflight Center, Greenbelt, Maryland, NASA SP-342.
Orrall, F. Q., and Zirker, J. B.: 1961, *Astrophys. J.* **134,** 72.
Orrall, F. Q., and Zirker, J. B.: 1963, in J. W. Evans (ed.), 'The Solar Corona', *IAU Symp.* **16.**
Parker, E. N.: 1958, *Astrophys. J.* **128,** 664.
Pneuman, G. W.: 1973, *Solar Phys.* **28,** 247.
Pneuman, G. W., and Kopp, R. A.: 1971, *Solar Phys.* **18,** 258.
Pneuman, G. W., and Kopp, R. A.: 1976, in preparation.
Webb, D. F., Krieger, A. S., and Rust, D. M.: 1976, *Solar Phys.* **48,** 159.